



Eidgenössische Technische Hochschule Zürich
Swiss Federal Institute of Technology Zurich



Empa

Materials Science and Technology

Thermomechanical Simulation for Distortion and Residual Stress Prediction in SLM Parts: a Sensitivity Analysis

Bachelor Thesis

Fabian Müller

June, 2021

Advisors: Prof. Dr. E.Mazza, Dr. E.Hosseini, P. Gh. Ghanbari

Experimental Continuum Mechanics, Empa
Department of Mechanical and Process Engineering, , ETH Zürich

Abstract

Unwanted distortions as a result of residual stress in metal additive manufacturing caused by the high local temperature gradients and cooling rates influence its efficiency strongly. Computationally efficient prediction methods for residual stress and strain are needed to simplify the complex multi physics phenomena. The inherent strain method is such a tool and has been used in literature and commercially available tools alike. In this work a sensitivity analysis with Ansys Additive Print 2020R2 is performed. It uses the inherent strain method for fast residual stress and distortion prediction. To investigate the implementation of inherent strain a control inherent strain model is implemented directly in Abaqus CAE.

Acknowledgements

First, I would like to thank Prof. Dr. Edoardo Mazza for the opportunity to do my bachelors thesis in the Experimental Continuum Laboratory. I also wish to thank Dr. Ehsan Hosseini and Pooriya Gh Ghanbari for the supervision of the project and the many helpful insights and discussions we had. They both were a great help during the project.

Further I would like to thank all HTIG group members for their inputs during the biweekly meetings and also Manfred Maurer from CADFEM for his insights in Ansys Additive Print.

Contents

Contents	iii
List of Figures	iv
List of Tables	v
1 Introduction	1
1.1 Motivation	1
1.2 Goal	2
2 Theory	3
2.1 Original inherent strain method	3
2.2 Inherent strain method in metal additive manufacturing	4
3 Inherent Strain Model	6
3.1 Ansys Additive Print 2020 R2	6
3.1.1 Cube model	8
3.2 Control Inherent Strain Model	10
3.2.1 Control cube model	10
4 Results	12
4.1 Comparison between AAP AS, SPS and TS	12
4.2 Comparison between AAP AS and Abaqus isotropic IS	14
4.3 Comparison between AAP SPS and Abaqus anisotropic IS	18
4.4 Sensitivity Analysis AAP	22
4.4.1 Assumed Strain	22
4.4.2 Scan Pattern Strain	22
4.4.3 Thermal Strain	25
5 Conclusion and Outlook	32

List of Figures

3.1	Effect of voxel size on geometrical simplification of model.	7
3.2	AAP cube model with stripe print strategy indicated on top layer.	9
3.3	Abaqus cube model with partitioned slices.	11
4.1	Comparison of AAP AS, SPS and TS on plate residual stress and displacement.	13
4.2	Comparison of AAP AS and Abaqus isotropic IS.	15
4.3	Comparison of on plate residual stress between AAP AS and Abaqus isotropic IS.	16
4.4	Comparison of on plate displacement between AAP AS and Abaqus isotropic IS.	17
4.5	Comparison between AAP SPS and Abaqus anisotropic IS.	19
4.6	Comparison of on plate residual stress between AAP SPS and Abaqus anisotropic IS.	20
4.7	Comparison of on plate displacement between AAP SPS and Abaqus anisotropic IS.	21
4.8	AAP AS sensitivity to voxel size.	23
4.9	AAP SPS sensitivity to layer thickness.	24
4.10	AAP TS sensitivity to laser scan speed.	26
4.11	AAP TS sensitivity to laser power.	27
4.12	AAP TS sensitivity to laser beam diameter.	29
4.13	AAP TS sensitivity to hatch spacing.	30
4.14	AAP TS sensitivity to base plate temperature.	31

List of Tables

3.1	Predefined material properties of IN718 in AAP.	9
3.2	Input parameters for the AAP AS, SPS and TS calculations.	9
3.3	Employed material parameters in Abaqus for representing isotropic IS analysis.	11
3.4	Employed material parameters in Abaqus for representing anisotropic IS analysis.	11

Introduction

1.1 Motivation

Additive manufacturing processes (AM) build parts by continuously building it in a layer by layer fashion [1]. The most common metal Additive Manufacturing processes (MAM), like laser or electron beam melting (LBM, EBM), are powder based approaches. With LBM and EBM a part is built out of a powder bed by multiple layers of micro welding seams. Other MAM technologies are laser cladding or powder deposition welding [2, 3]. Nonetheless, most MAM technologies share the same basic principle of melting a metallic material and its subsequent solidification. The melting of material in MAM is achieved with different heat sources with high local energy densities which result in high cooling rates and temperature gradients during the build process [3]. High thermal strains and residual stresses are created in the built part. These residual stresses and strains cause unwanted distortions for example during the cutting of support structures through redistribution to a new equilibrium [3, 4]. Unwanted distortions are a critical factor of MAM, since they increase manufacturing costs, times and generate unusable scrap parts. Often corrective measures can only be applied after production through a trial and error approach. An experimental approach that lacks flexibility and cost efficiency. Alternatively, preventive methods based on numerical methods can predict distortions in the design phase already and be a powerful tool for part design and optimization [5, 6]. Although being a relatively new field there have already been introduced many MAM simulation approaches in Literature [6]. The different approaches differ in the physical phenomena considered and numerical methods applied. Micro scale models considering complex multi physics phenomena can simulate many process related thermo-fluid dynamic effects but require extensive computational power and use non standard numerical methods. Therefore, only small domains are practical (a few ms and a fraction of mm^3) [6, 7]. A different approach is the continuum thermo-mechanical finite element method (FEM). Through the

definition of thermo-mechanical properties of the used material, it is possible to find stress and strain states at each time step. But again the computational power for part size calculations is impractical and therefore not applicable to bigger models [6, 8]. For the simulation of part size models therefore it is necessary to reduce the computational power drastically [3, 5, 6]. Two different approaches have been used so far. The inherent strain (IS) method and the equivalent scanning method. With the IS method the thermal stress build up through the production is implemented with a strain tensor that is activated in a model in a layer wise fashion [3, 6]. The equivalent scanning method applies a representative surface or body heat flux to a target volume or entire layer [6].

1.2 Goal

In this work a sensitivity analysis for the commercially available Ansys Additive Print 2020 R2 software is conducted and the implementation of IS investigated using a control IS model set up in Abaqus CAE.

Chapter 2

Theory

2.1 Original inherent strain method

Originally the IS method was introduced in welding mechanics to reduce calculation time of large welding problems such as steel ship hulls [9, 10]. Generally in welding mechanics the total strain in an element in the weld seam can be decomposed as follows:

$$\varepsilon = \varepsilon^{el} + \varepsilon^p + \varepsilon^t + \varepsilon^c + \varepsilon^{tr} \quad (2.1)$$

where ε is the total strain, ε^{el} the elastic strain, ε^p the plastic strain, ε^t the thermal strain, ε^c the creep strain and ε^{tr} the strain produced by phase transformation [11]. After welding the elastic strain in a weld seam is released. Therefore, the residual stress in a single seam weld is the result of plastic strain, thermal strain of the weld metal, creep strain and strain due to phase transformation [12]. The IS is defined as the difference between the total strain ε and the elastic strain ε^{el} .

$$\varepsilon^* = \varepsilon - \varepsilon^{el} = \varepsilon^p + \varepsilon^t + \varepsilon^c + \varepsilon^{tr} \quad (2.2)$$

Since only the final cooled state of the weld is considered in the original IS theory usually the thermal strain ε^t , the creep strain ε^c and strain due to phase transformation ε^{tr} are neglected [13].

$$\varepsilon^* = \varepsilon^p \quad (2.3)$$

Using this convenient definition the components of the IS tensor caused in a welding problem can be found easily either by a short single bead thermo-mechanical FEM analysis or directly measured from welding experiments [14]. Through measurements of the residual strain in a weld seam at different points the inverse IS problem can be formulated to find the IS tensor [15].

Under the assumption that the weld seams in large parts show a similar thermal history the found IS is applied as initial strain in the heat affected zone (HAZ) of the weld region to calculate the distortion in a static FEM analysis [14].

2.2 Inherent strain method in metal additive manufacturing

In the work of Keller et al. [3] the original IS method is directly applied to a LBM process under the assumption that the process is in fact a layer by layer micro multi pass weld. The characteristic IS is found through a multi scale calculation approach. A small scale thermo-mechanical analysis simulates the laser passing over a small hatching region to calculate the IS tensor. The found IS is then applied to a macro model in a layer by layer fashion [3]. However the work of Bugatti et al. [6] showed that the prediction capabilities of this approach are very poor. The output of the MAM layer by layer IS model completely rely on the computed IS values of the small-scale thermo-mechanical simulation which can have high uncertainties due to the difficulty of capturing the temperature dependent material properties correctly [6]. Bugatti et al. [6] showed that the results can be improved by implementing a hybrid experimental-numerical approach were the IS tensor is found through a regression based optimization problem.

Although the original IS method can be directly implemented in MAM and produce reasonable results using accurate IS values, the original theory makes simplifications that do not necessarily hold in the context of MAM. In the work of Liang et al. [16] a modified IS method is introduced to capture the nature of the layer by layer effect in MAM. Other than in a single pass weld in MAM the assumption of the elastic strain being fully released after cooling to ambient temperature does not hold for MAM since the newly formed layers act as a mechanical constraint on layers beneath it. Therefore the assumption that the IS is only composed of the plastic strain ϵ^p is invalid and has to be adjusted to also consider elastic strains ϵ^{el} arising due to the layer by layer shrinkage during the cooling process coupled with the inter layer constraint of newly added layers. The modified IS is defined using an intermediate and steady state characteristic for MAM processes. The intermediate state is defined as the state when the heat source just passes by an element and the local (compressive) mechanical strain reaches the largest amplitude due to large thermal expansion. The steady state is defined as the state of the element after cooling to ambient temperature.

2.2. Inherent strain method in metal additive manufacturing

The modified IS is defined as the difference between the total mechanical strain at the intermediate state and the elastic strain at the steady state [13, 14].

$$\varepsilon_{modified}^* = \varepsilon_{intermediate}^{pl} + \varepsilon_{intermediate}^{el} - \varepsilon_{steadystate}^{el} \quad (2.4)$$

The modified IS shows a far better distortion prediction for MAM than the original theory. Liang et al. [14, 13] investigated a IN718 double cantilever beam with the calculated distortion having an error of less than 10% using the modified inherent strain method implemented in a multiscale approach similar to the work of Keller et al. [14].

Inherent Strain Model

3.1 Ansys Additive Print 2020 R2

Ansys Additive Print (AAP) is a interface offered by Ansys that provides different MAM simulation possibilities. The simulation methods use a layer by layer accumulation of IS to predict distortion and residual stress during the build. Other possible outputs are for example displacement after support cutoff or possible recoater blade crash warnings. Three different calculation modes can be chosen that differ in accuracy and calculation time. These are assumed strain (AS), scan pattern strain (SPS) and thermal strain (TS). A voxelisation method is used to mesh a part whereas a voxel is a 8 Node hexahedral element. AAP uses a calibration approach to estimate the IS apparent in a build [17]. Following an overview of the most important aspects of AAP is given. For an in depth explanation see AAP user guide [17].

Assumed Strain

The AS calculation mode assumes an isotropic IS that is activated in each voxel of a build layer. The IS is equal to the strain scaling factor (SSF) multiplied by yield strength and divided by elastic modulus. Whereas the SSF is found through a calibration step [17].

$$\epsilon^* = SSF * \sigma_{\text{yield}} / E \quad (3.1)$$

Scan Pattern Strain

In the SPS calculation mode the same IS ϵ^* is implemented as in AS but isotropy is no longer assumed. The IS tensor is corrected with respect to the scan pattern applied in the build. For each voxel the average scan vector is evaluated and the IS tensor rotated to align the individual scan direction of

each voxel. With the three anisotropic strain coefficients (ASF) it accounts for the effect that in the direction of the scan path more strain is apparent than in the perpendicular and out of plane build direction. The ASF are also found through a calibration step [17].

$$\varepsilon_{\parallel}^* = ASF_{\parallel} * \varepsilon^* \quad (3.2)$$

$$\varepsilon_{\perp}^* = ASF_{\perp} * \varepsilon^* \quad (3.3)$$

$$\varepsilon_z^* = ASF_z * \varepsilon^* \quad (3.4)$$

Thermal Strain

Other than in AS and SPS in the TS calculation mode thermal cycling effects are also considered in the simulation. The thermal ratcheting algorithm assigns a base strain for each individual voxel as it solidifies. If already solidified voxels are heated above a threshold of 40% of the liquidus temperature the base strain is increased by an unknown amount. In case of remelting the base strain is reset. The found strain is passed on as ε^* to the mechanical solver and implemented as inherent strain through the SSF and ASF factors similarly as in the SPS calculation mode [17].

Voxelisation

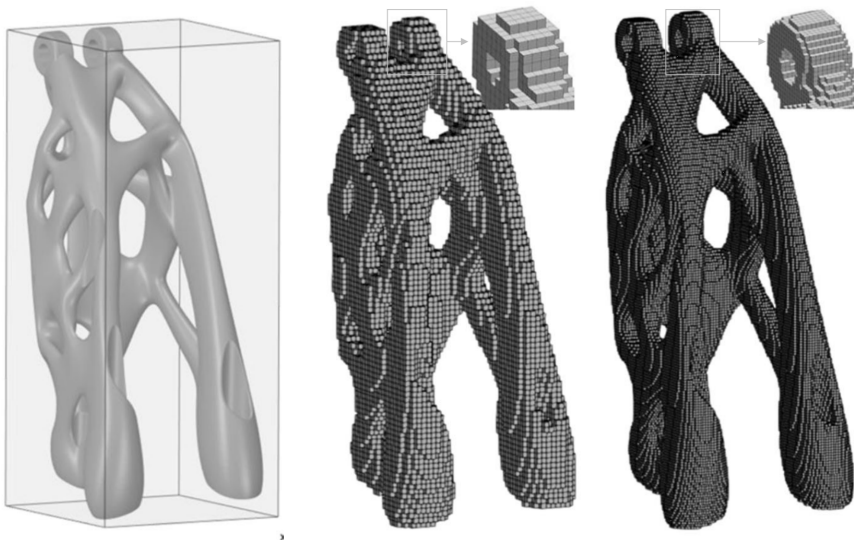


Figure 3.1: Effect of voxel size on geometrical simplification of model [18].

Before the mechanical analysis the geometry of a part is simplified using cubic voxels and meshed with 8 node hexahedral elements of the same size. Figure 3.1 illustrates the effect of voxel size on geometrical simplification of a part. The voxel size has a direct impact on the implementation of IS since it defines the thickness of the layers to which the IS is applied. Generally the voxel size should be at least 1/4 of the smallest feature size [17].

Material model

Either an elastic or elastoplastic material model can be chosen for all three calculation modes. For the elastoplastic material model AAP considers a von mises J2 flow criterion with linear hardening rule. The slope of the linear hardening rule E_t is parametrised through the user defined hardening factor μ [17].

$$E_t = \mu * E \quad (3.5)$$

Calibration

AAP uses an iterative approach to define the IS in a build. It is assumed that the same powder properties and machine parameters give a unique IS independent of printed geometry. Therefore a simple calibration geometry can be used to experimentally find the IS. In the first iteration the distortion of the calibration geometry for example a cantilever beam is calculated in the intended calculation mode with $SSF = 1, ASF_{\parallel} = 1.5, ASF_{\perp} = 0.5$ and $ASF_z = 1$ and compared with the distortion of the printed calibration geometry. In the following iterations the SSF and ASF factors are adjusted that the simulated distortions fit the measured distortions. The found SSF and ASF factors are then used in the actual simulation [16].

3.1.1 Cube model

For the sensitivity analysis of the three calculation modes a simple 2x2x2mm IN718 cube has been setup in AAP with a simple stripe print strategy as indicated in figure 3.2. The SSF and ASF are set to the arbitrary values of $SSF = 1, ASF_{\parallel} = 1.5, ASF_{\perp} = 0.5$ and $ASF_z = 1$. Therefore the solutions are not expected to give a realistic prediction of the actual residual stress or strains but to give insight on trends with changes in input parameters. Following the parameters for the three calculation modes are listed.

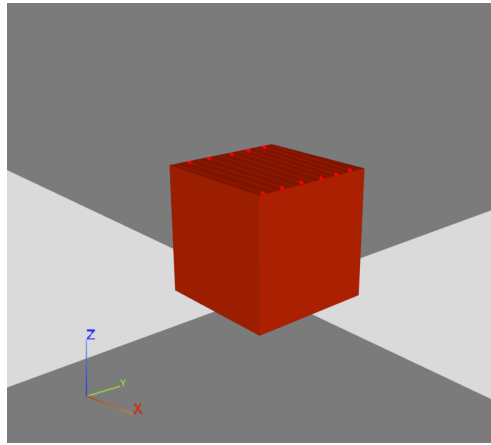


Figure 3.2: AAP cube model with stripe print strategy indicated on top layer.

Material Property	value
Material	IN718
Stress Mode	J2 Plasticity
Load Stepping Type	Dynamic Load Stepping
Hardening factor	0.0048
Elastic Modulus [GPa]	211000
Poisson Ratio	0.3
Yield Point [MPa]	1040

Table 3.1: Predefined material properties of IN718 in AAP.

Parameter	AS	SPS	TS
Voxel Size [mm]	0.1	0.1	0.1
SSF	1	1	1
ASF_{\parallel}	-	1.5	1.5
ASF_{\perp}	-	0.5	0.5
ASF_z	-	1	1
layer Thickness [μm]	-	20	20
Hatch Spacing [μm]	-	-	100
Laser Power [W]	-	-	300
Scan Speed [mm/s]	-	-	1000
Laser Beam Diameter [μm]	-	-	100
Base Plate Temperature [$^{\circ}\text{C}$]	-	-	80

Table 3.2: Input parameters for the AAP AS, SPS and TS calculations.

3.2 Control Inherent Strain Model

To investigate if the implementation of IS in the AAP follows the understanding of IS implementation found in literature a control IS model has been set up in Abaqus CAE using the equivalent thermal expansion method and layer wise activation.

Equivalent thermal expansion

To achieve the intended IS in each element of a layer the thermal expansion coefficient α of the material is defined equal to the IS intended and a unitary temperature increase is applied. This way both isotropic and anisotropic IS can be applied to a model [6].

$$\alpha_* = \varepsilon_* \quad (3.6)$$

or in the case of anisotropic IS

$$\alpha_{11*} = \varepsilon_{11*} \quad (3.7)$$

$$\alpha_{22*} = \varepsilon_{22*} \quad (3.8)$$

$$\alpha_{33*} = \varepsilon_{33*} \quad (3.9)$$

Layerwise activation

To simulate the additive process layers are sequentially activated and given IS through unitary temperature increase. Initially all layers are deactivated using the model change feature in Abaqus CAE and then reactivated one layer after another.

3.2.1 Control cube model

A similar 2x2x2mm IN718 cube as in AAP has been set up. Two different cases have been considered. One with an isotropic IS definition similar to AAP AS and another considering anisotropic IS similar to AAP SPS. For the anisotropic model the same stripe print strategy in x direction without rotation between layers as in AAP SPS analysis is assumed. Therefore the average scan direction of each element is equal to the x coordinate direction. The cube is partitioned in 0.1mm layers and meshed with 0.1mm C3D8R elements corresponding to the voxel layers in AAP as shown in figure 3.3. The following tables give an overview of the used parameters.

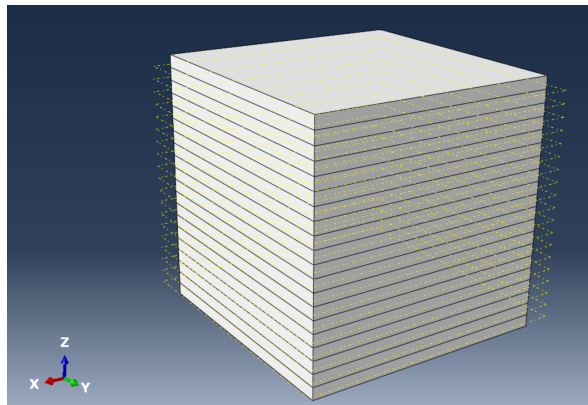


Figure 3.3: Abaqus cube model with partitioned slices.

properties isotropic model	
parameter	value
Elastic Modulus E [MPa]	211 000
Poisson Ratio ν	0.3
Yield Stress σ [Mpa]	1040
Hardening Rule	isotropic
Tangent modulus E_t [MPa]	1.012
Thermal Expansion Coefficient α	-0.004928

Table 3.3: Employed material parameters in Abaqus for representing isotropic IS analysis.

Properties anisotropic model	
parameter	value
Elastic Modulus [MPa]	211 000
Poisson Ratio	0.3
Yield Stress [Mpa]	1040
Hardening Rule	isotropic
Tangent Modulus E_t [MPa]	1.012
Thermal Expansion Coefficient	
α_{xx}	-0.00739
α_{yy}	-0.00246
α_{zz}	-0.004928

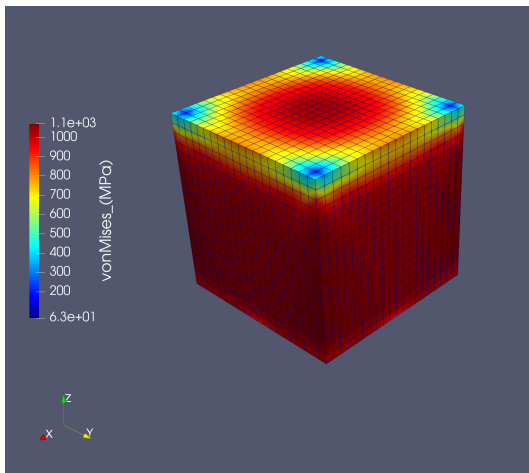
Table 3.4: Employed material parameters in Abaqus for representing anisotropic IS analysis.

Results

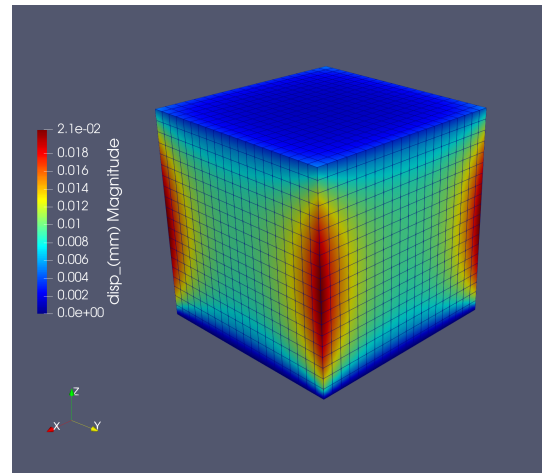
4.1 Comparison between AAP AS, SPS and TS

In Figure 4.1 the on plate residual stress and displacement of the three AAP calculation modes are shown. Whereas on plate refers to the cube still being attached to the build plate. A few qualitative aspects corresponding to the different implementations of IS in the calculation modes can be observed. AAP AS gives a symmetric solution to both the x and y plane corresponding to the isotropic character of the IS tensor. The solution of AAP SPS on the other hand is only symmetric to the y plane. Since the scan pattern used is always aligned in x direction $\varepsilon_{xx}^* > \varepsilon_{yy}^*$ holds for all voxels and leads to a larger build up of strain in the x direction. For the case of TS the same influence of the scan pattern regarding the symmetry of the solution is apparent. In addition the thermal ratcheting algorithm increases the inherent strain in some points. Due to the calculation not being calibrated it is difficult to interpret voxels with elevated IS through the thermal ratcheting algorithm.

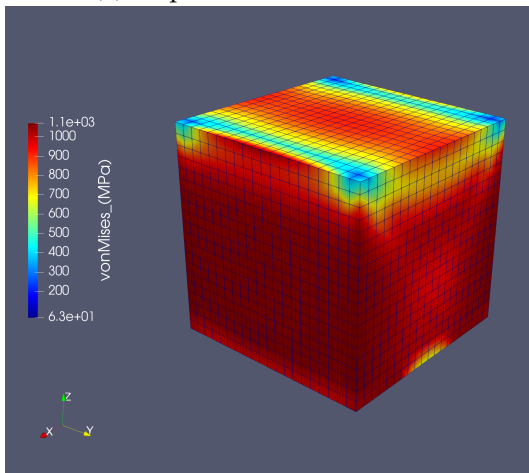
4.1. Comparison between AAP AS, SPS and TS



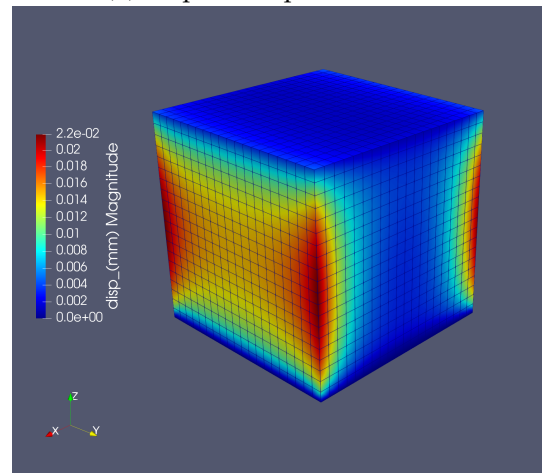
(a) on plate residual stress AS



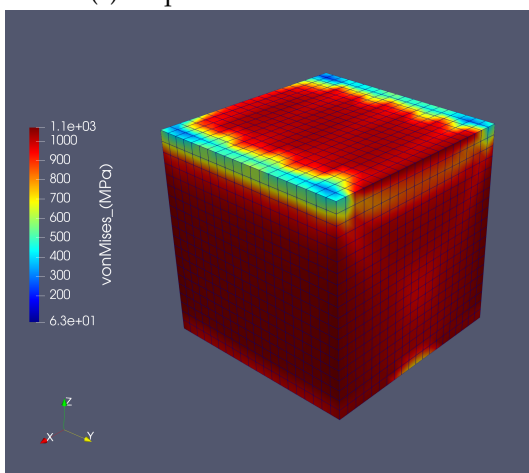
(b) on plate displacement AS



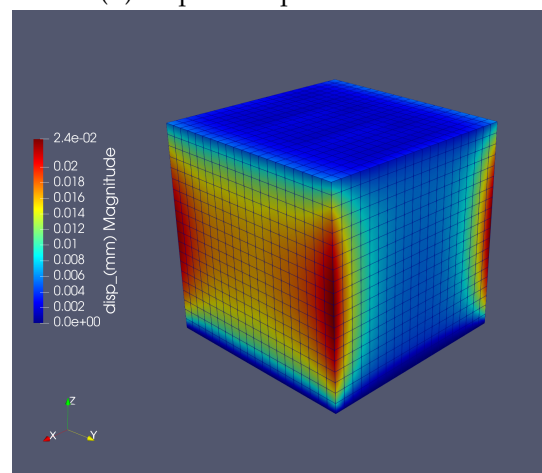
(c) on plate residual stress SPS



(d) on plate displacement SPS



(e) on plate residual stress TS



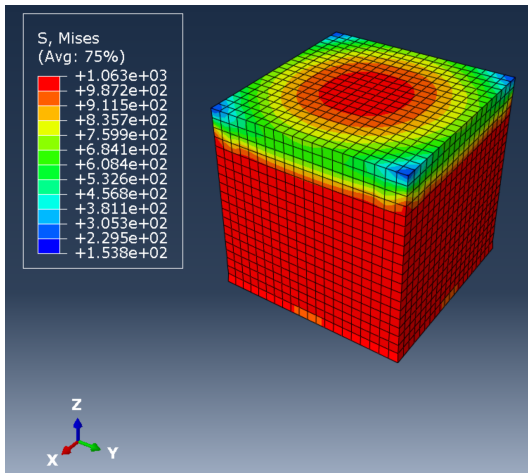
(f) on plate displacement TS

Figure 4.1: Comparison of AAP AS, SPS and TS on plate residual stress and displacement.

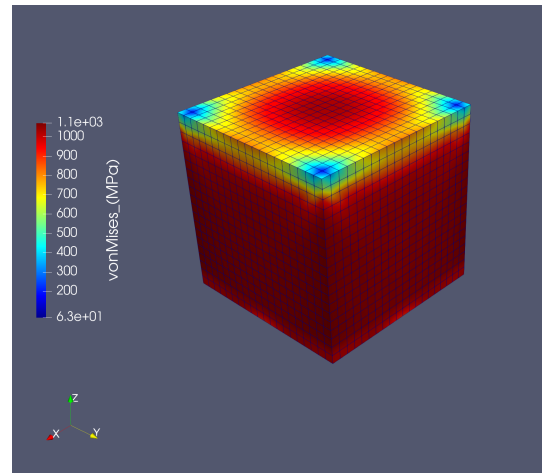
4.2 Comparison between AAP AS and Abaqus isotropic IS

In Figure 4.2 the on plate residual stress and displacement of the AAP AS calculation is compared with the control isotropic IS model setup in Abaqus CAE. Qualitatively the two solutions match regarding on plate residual stress and displacement very well. To quantitatively compare both calculations characterising stress/displacement features are investigated. By cutting the cube through the y symmetry plane a characteristic tooth shaped stress field is found (Fig.4.2 (c) and (d)). For the displacements the outer edges of the cube are considered. Figure 4.3 and Figure 4.4 show the on plate residual stress and displacement of the control IS calculation plotted over lines through each characteristic feature. The on plate residual stress and displacement of both models match very well for all but the first two layers. In Figures 4.4 (a), (b), and (c) the displacement data shows non smooth results. This might be a computational instability due to high strains applied to very thin material in the first layers. Another possible source of error is that the extracted values are extrapolated from the integration point which can be problematic at free surfaces.

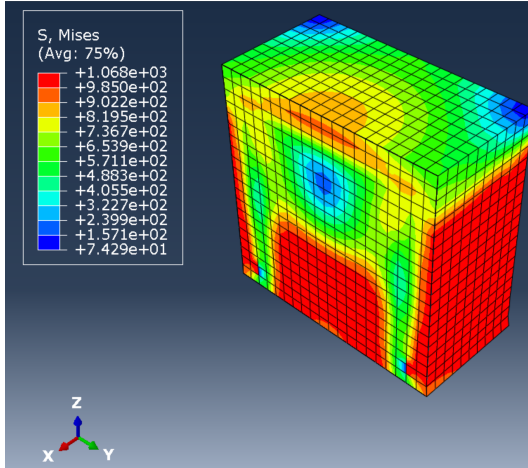
4.2. Comparison between AAP AS and Abaqus isotropic IS



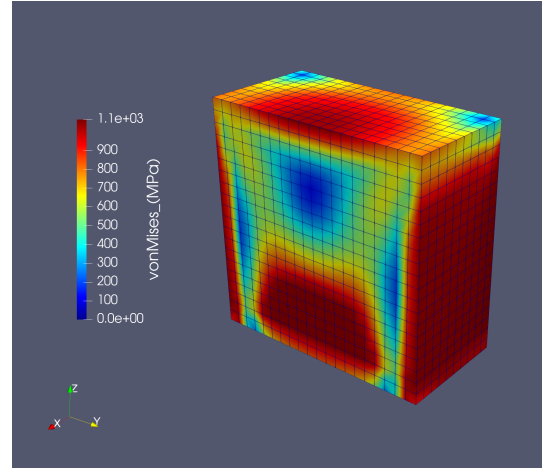
(a) on plate residual stress control isotropic IS



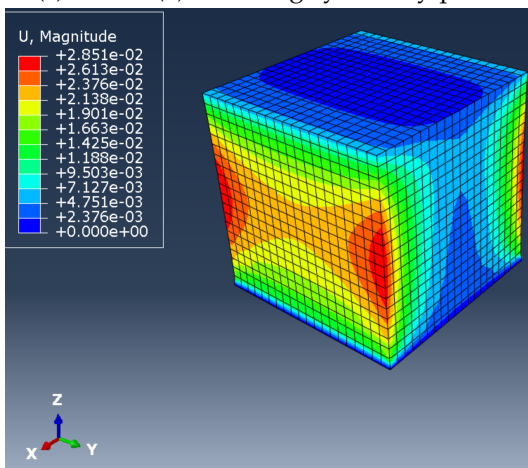
(b) on plate residual stress AAP AS



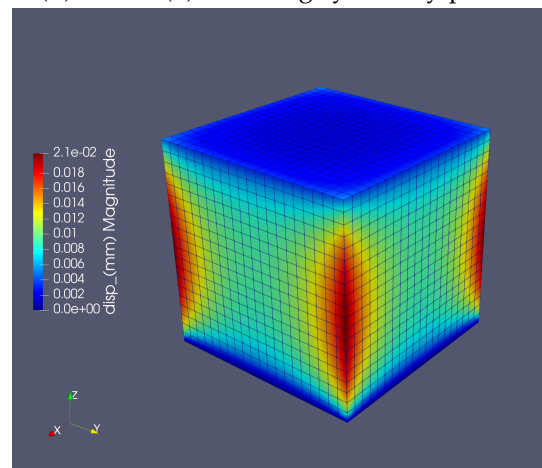
(c) model (a) cut along symmetry plane



(d) model (b) cut along symmetry plane



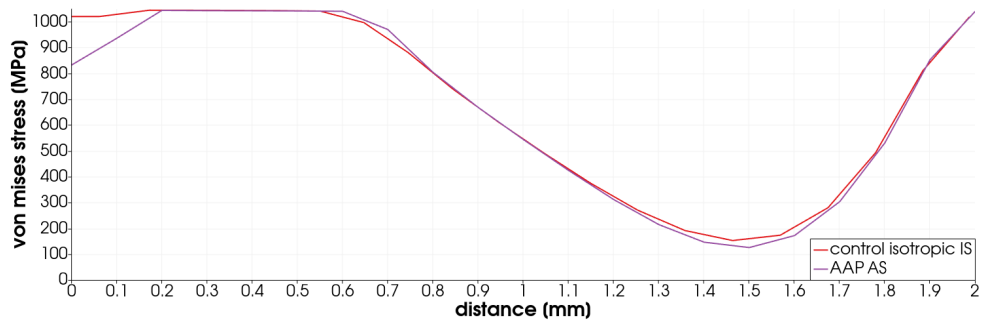
(e) on plate displacement control isotropic IS



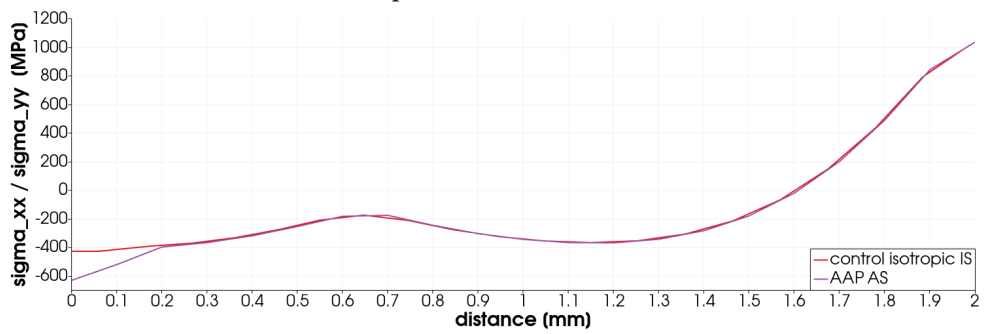
(f) on plate displacement AAP AS

Figure 4.2: Comparison of AAP AS and Abaqus isotropic IS.

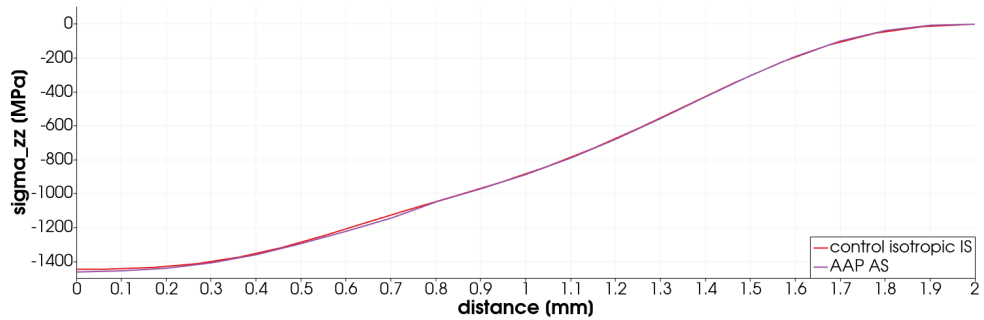
4. RESULTS



(a) von mises stress plotted over line from [1,1,0] to [1,1,2]



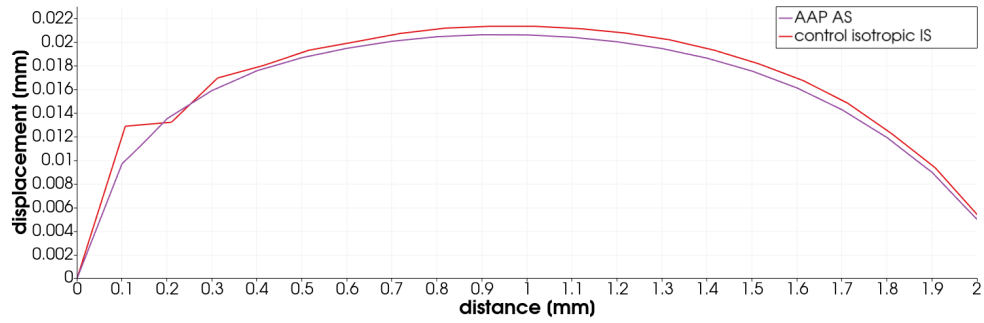
(b) $\sigma_{xx} = \sigma_{yy}$ plotted over line from [1,1,0] to [1,1,2]



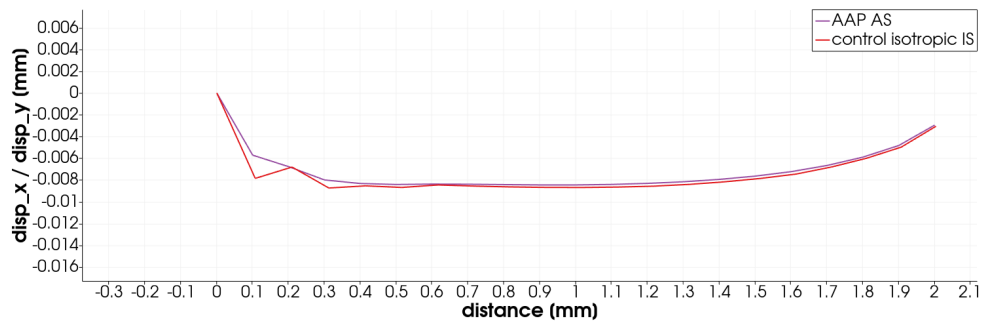
(c) σ_{zz} plotted over line from [1,1,0] to [1,1,2]

Figure 4.3: Comparison of on plate residual stress between AAP AS and Abaqus isotropic IS.

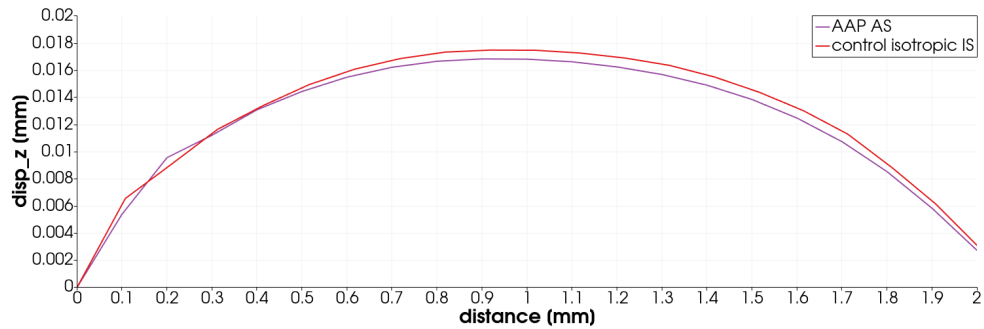
4.2. Comparison between AAP AS and Abaqus isotropic IS



(a) on plate displacement magnitude plotted over line from [2,2,0] to [2,2,2]



(b) on plate x-displacement=y-displacement plotted over line from [2,2,0] to [2,2,2]



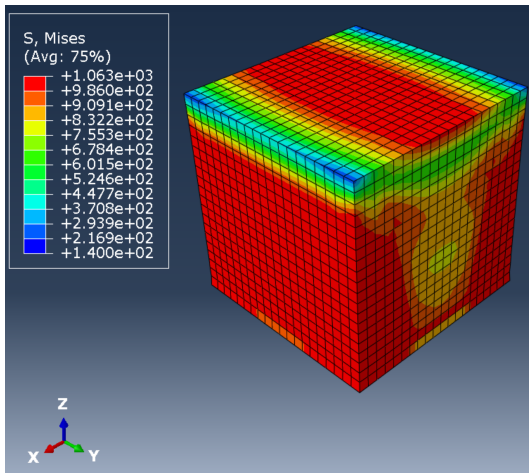
(c) on plate z-displacement plotted over line from [2,2,0] to [2,2,2]

Figure 4.4: Comparison of on plate displacement between AAP AS and Abaqus isotropic IS.

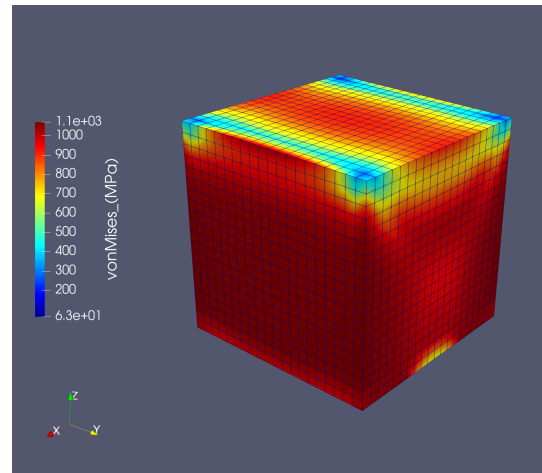
4.3 Comparison between AAP SPS and Abaqus anisotropic IS

Figure 4.5 shows the on plate residual stress and displacement of the AAP SPS calculation compared with the control anisotropic IS model setup in Abaqus CAE. Same as in the case for isotropic IS qualitatively the two solutions match regarding on plate residual stress and displacement very well. To quantitatively compare both calculations the same characterizing features as for the isotropic case are investigated. Figure 4.5 (b),(c),(d) and (e) show the considered tooth shaped stress field when the cube is cut as well as the displacement of the cubes outer edge. Considering the data in figures 4.7 and 4.6 also quantitatively the two models compare well. Overall the general shape of the residual stress and displacement plots fit well. Although in figure 4.7 (b) and (c) the curves show an offset and the same numerical issues already found in the isotropic case. However, the data of both the isotropic and anisotropic case appear sufficient to confirm that the implementation of IS in AAP follows the principles of the original IS method found in literature.

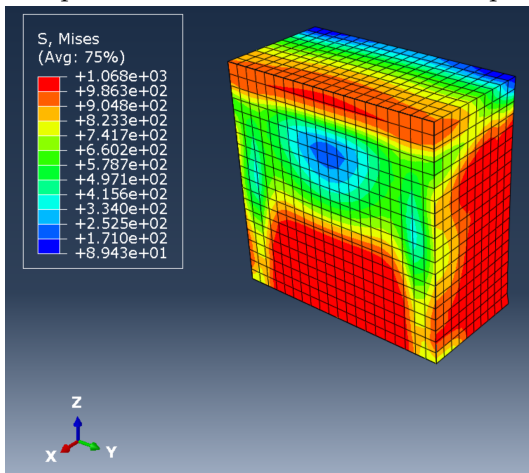
4.3. Comparison between AAP SPS and Abaqus anisotropic IS



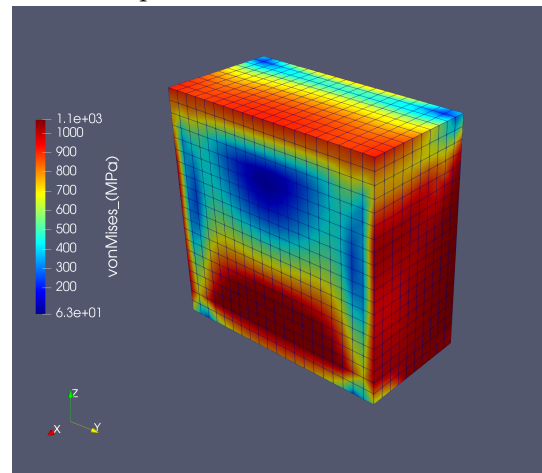
(a) on plate residual stress control anisotropic IS



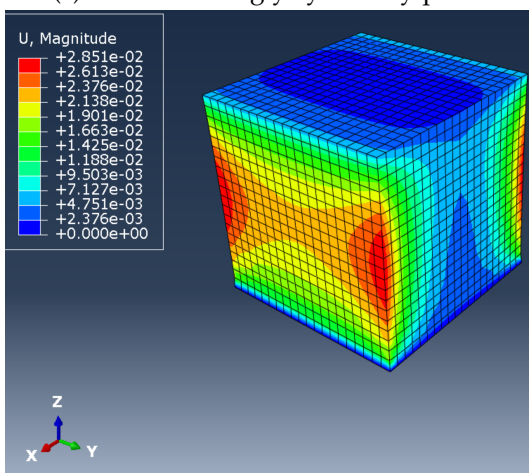
(b) on plate residual stress AAP SPS



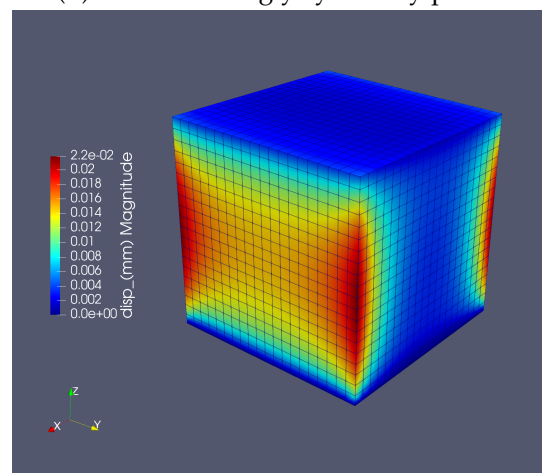
(c) cut view along y symmetry plane



(d) cut view along y symmetry plane



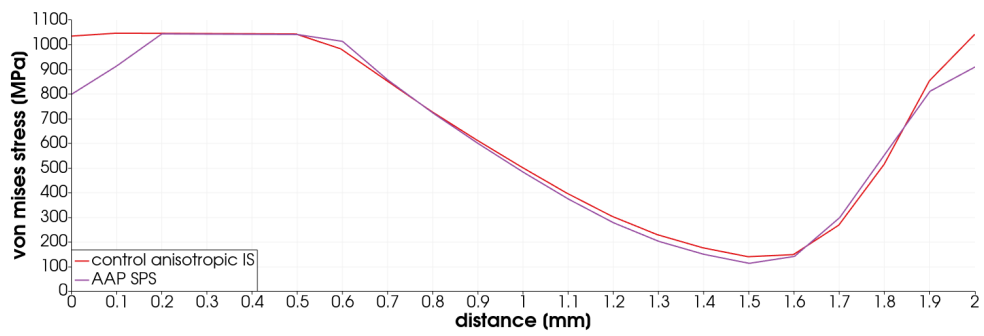
(e) on plate displacement control anisotropic IS



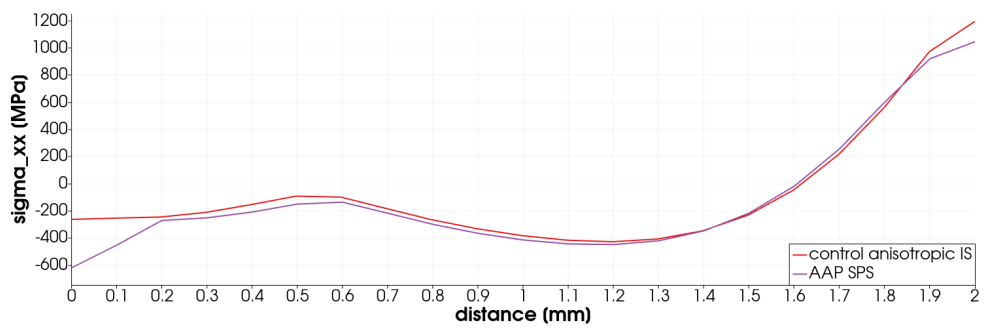
(f) on plate displacement AAP SPS

Figure 4.5: Comparison between AAP SPS and Abaqus anisotropic IS.

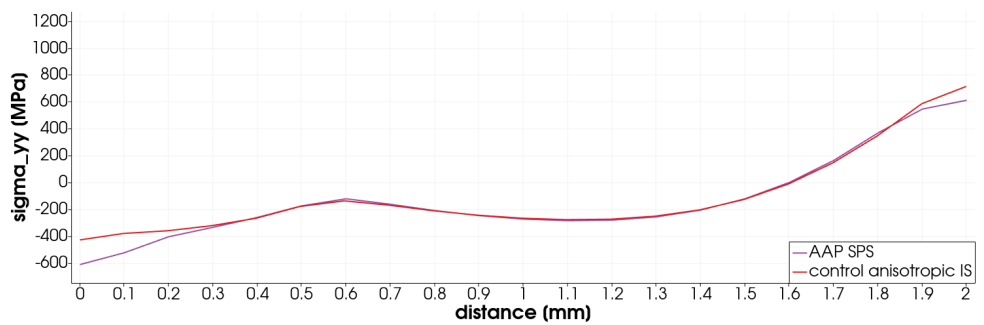
4. RESULTS



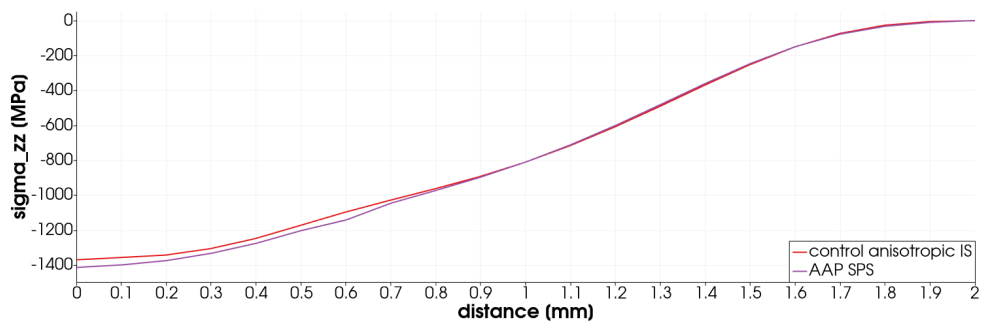
(a) von mises stress plotted over line from [1,1,0] to [1,1,2]



(b) σ_{xx} plotted over line from [1,1,0] to [1,1,2]



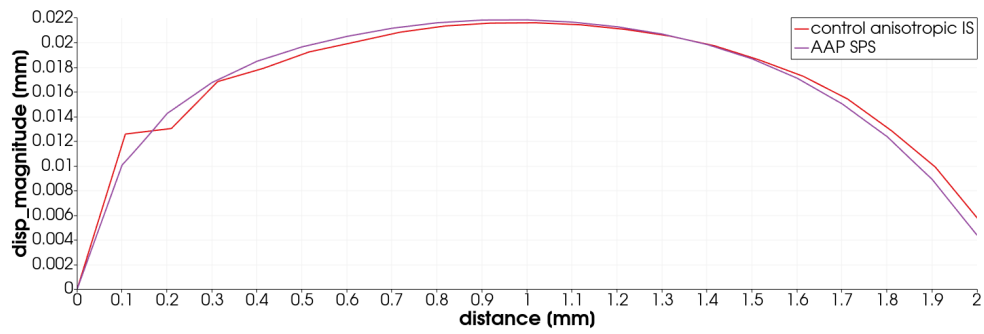
(c) σ_{yy} plotted over line from [1,1,0] to [1,1,2]



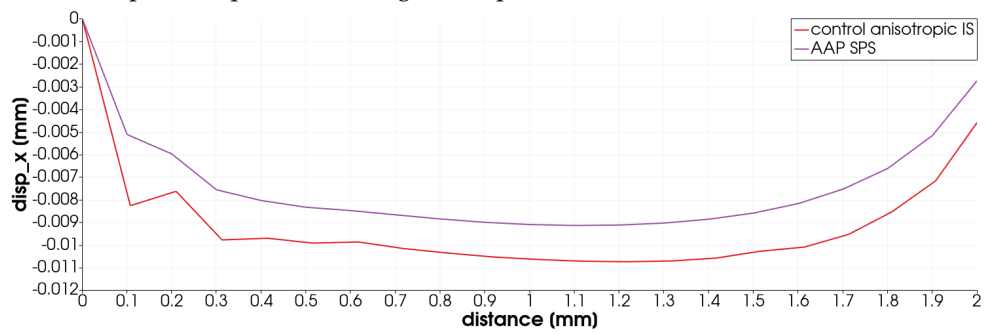
(d) σ_{zz} plotted over line from [1,1,0] to [1,1,2]

Figure 4.6: Comparison of on plate residual stress between AAP SPS and Abaqus anisotropic IS.

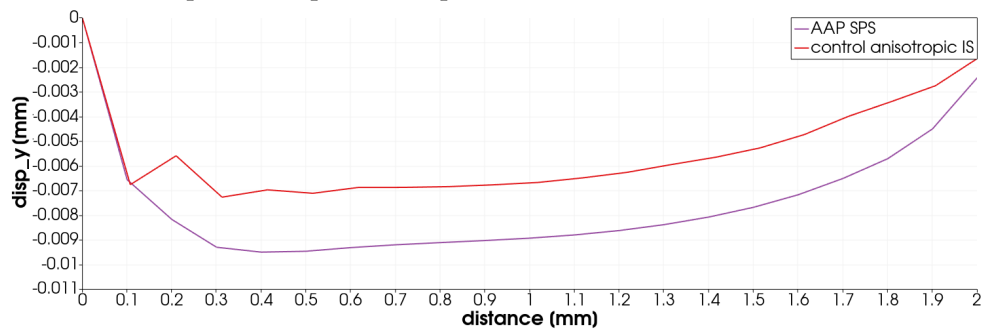
4.3. Comparison between AAP SPS and Abaqus anisotropic IS



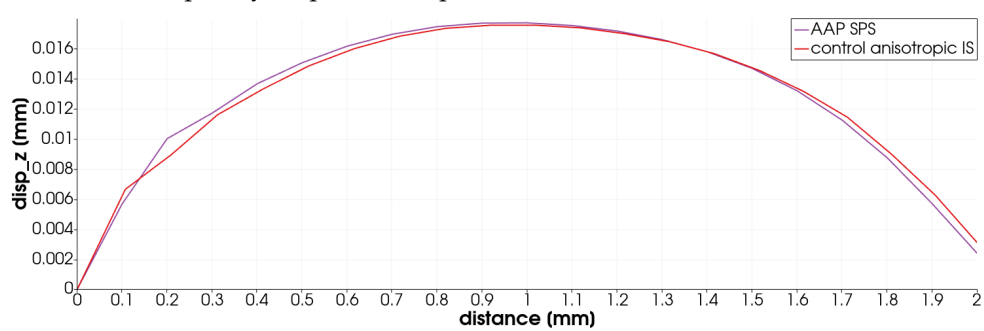
(a) on plate displacement magnitude plotted over line from [2,2,0] to [2,2,2]



(b) on plate x-displacement plotted over line from [2,2,0] to [2,2,2]



(c) on plate y-displacement plotted over line from [2,2,0] to [2,2,2]



(d) on plate z-displacement plotted over line from [2,2,0] to [2,2,2]

Figure 4.7: Comparison of on plate displacement between AAP SPS and Abaqus anisotropic IS.

4.4 Sensitivity Analysis AAP

For the sensitivity analysis of the three AAP calculation modes the on plate residual stress and displacement have been investigated along the two characteristic stress and strain fields described in chapter 4.2.

4.4.1 Assumed Strain

Voxel sensitivity

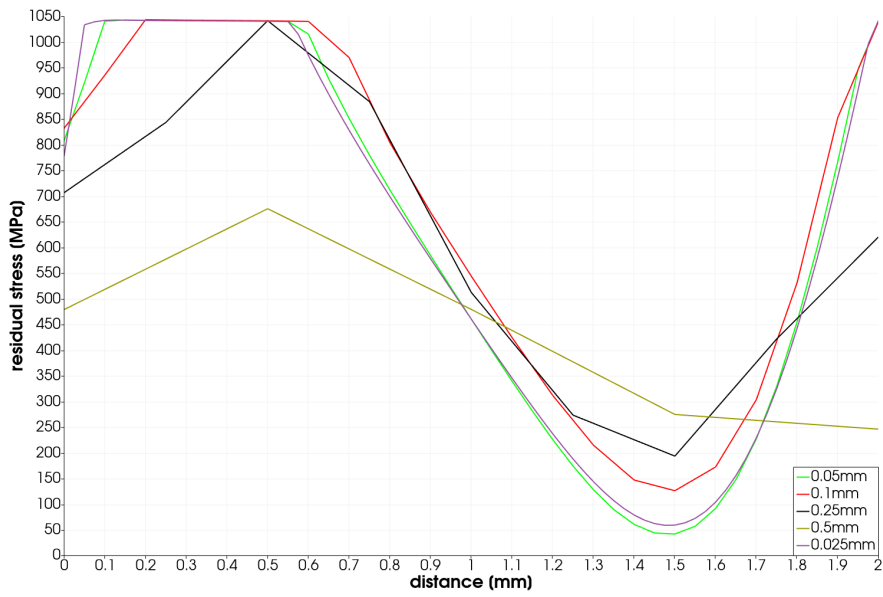
The initial voxel size of 0.1mm has been changed to the following set of values [0.5mm , 0.25mm , 0.05mm , 0.025mm]. Figure 4.8 (a) and (b) shows voxel size significantly influences both on plate residual stress and displacement. It can be seen that with a voxel size of 0.5mm and 0.25mm the characteristic residual stress and displacement curves are not captured. For the voxels of size 0.1mm , 0.05mm and 0.025mm a converging solution is found showing the same characteristics. The calculation time was 1 minute for the 0.1mm voxel, 8 minutes for the 0.025mm voxel and 2 hours for the 0.025mm voxel. A 0.1mm voxel is a good trade off since it captures the general characteristic and calculates quickly.

4.4.2 Scan Pattern Strain

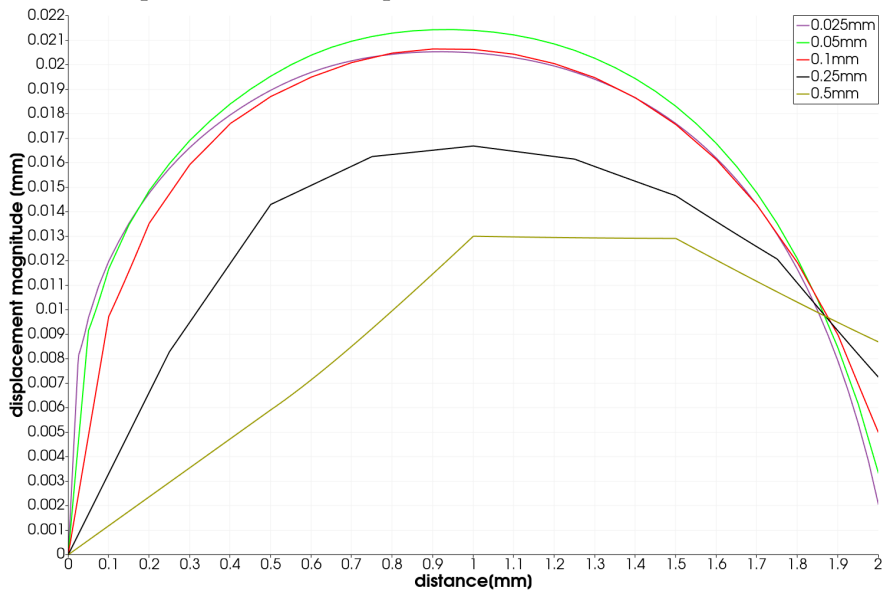
Layer thickness

The initial layer thickness of $20\mu\text{m}$ has been increased to $30\mu\text{m}$ as well as decreased to $10\mu\text{m}$. Figure 4.9 (a) and (b) show no sensitivity to layer thickness in regards to on plate residual stress and displacement. Since the scan vectors are all aligned in the x coordinate direction the average direction of each voxel will stay the x direction independent of layer thickness and result in the same IS applied to each voxel.

4.4. Sensitivity Analysis AAP



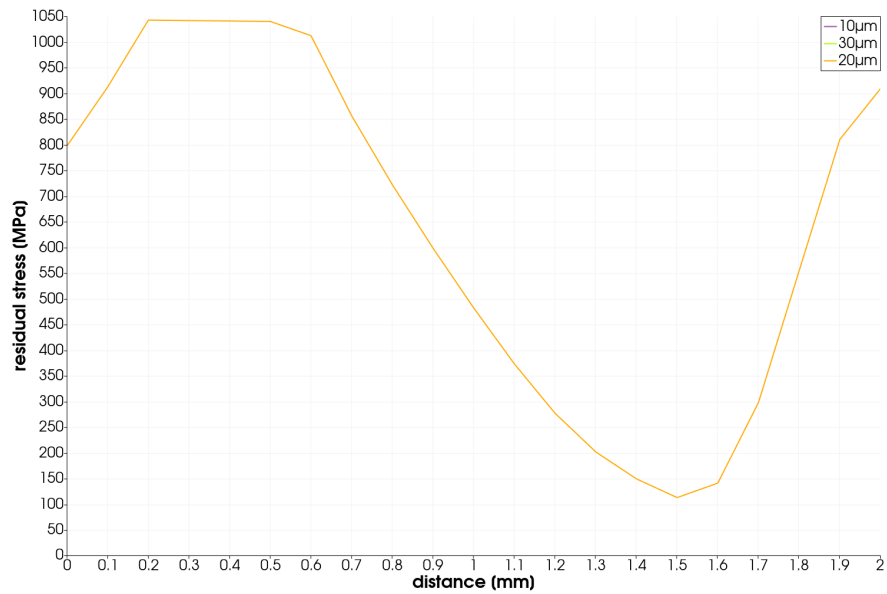
(a) on plate residual stress plotted over line from [1,1,0] to [1,1,2]



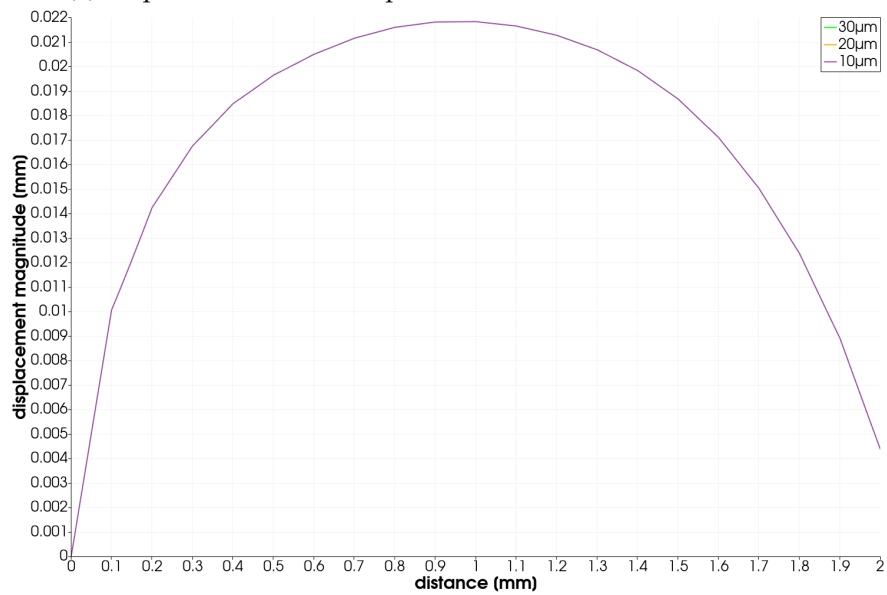
(b) on plate displacement plotted over line from [2,2,0] to [2,2,2]

Figure 4.8: AAP AS sensitivity to voxel size.

4. RESULTS



(a) on plate residual stress plotted over line from [1,1,0] to [1,1,2]



(b) on plate displacement plotted over line from [2,2,0] to [2,2,2]

Figure 4.9: AAP SPS sensitivity to layer thickness.

4.4.3 Thermal Strain

For the sensitivity analysis of the TS parameters it has to be noted that changing machine parameters would demand a recalibration of the SSF and ASF since these are seen as unique for the set of real print parameters. In the TS sensitivity analysis however a single parameter has been changed with the rest of the parameters being constant. Therefore, the results can not be expected to be physically meaningful but trends regarding the application of the thermal ratcheting algorithm can still be investigated. Each input parameter has been varied with an increased and decreased value and its sensitivity to on plate residual stress and displacement investigated.

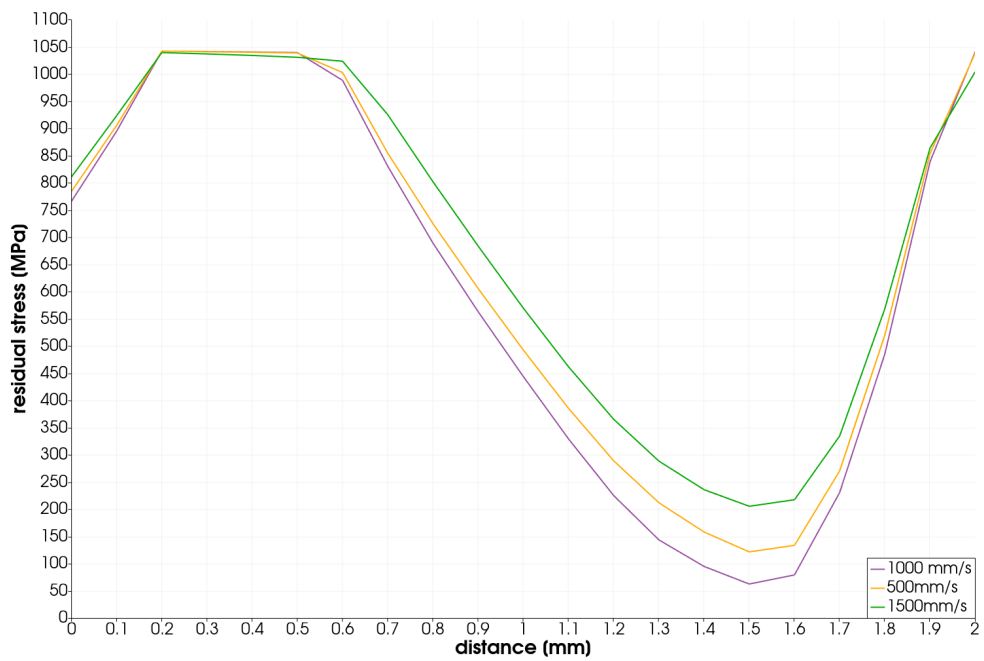
Laser scan speed

The initial laser scan speed of 1000mm/s has been increased to 1500mm/s as well as decreased to 500mm/s . Figure 4.10 (a) shows that the laser scan speed affects the on plate residual stress where the material does not yield strongly. However, no clear trend regarding residual stress and change in laser scan speed is apparent. Figure 4.10 (b) shows that the on plate displacement is also sensitive to changes in laser scan speed. Vastola et al. [19] found that with decreasing the laser scan speed or laser power in a thermo-mechanical single track EBM FEM model the HAZ decreases. A possible explanation that the laser scan speed of 500mm/s shows the smallest on plate displacement is that through the larger HAZ the IS of more voxels is reset due to remelting at some point during the build. Whereas with a higher laser scan speed the same voxels are still given elevated IS values resulting in an overall higher distortion.

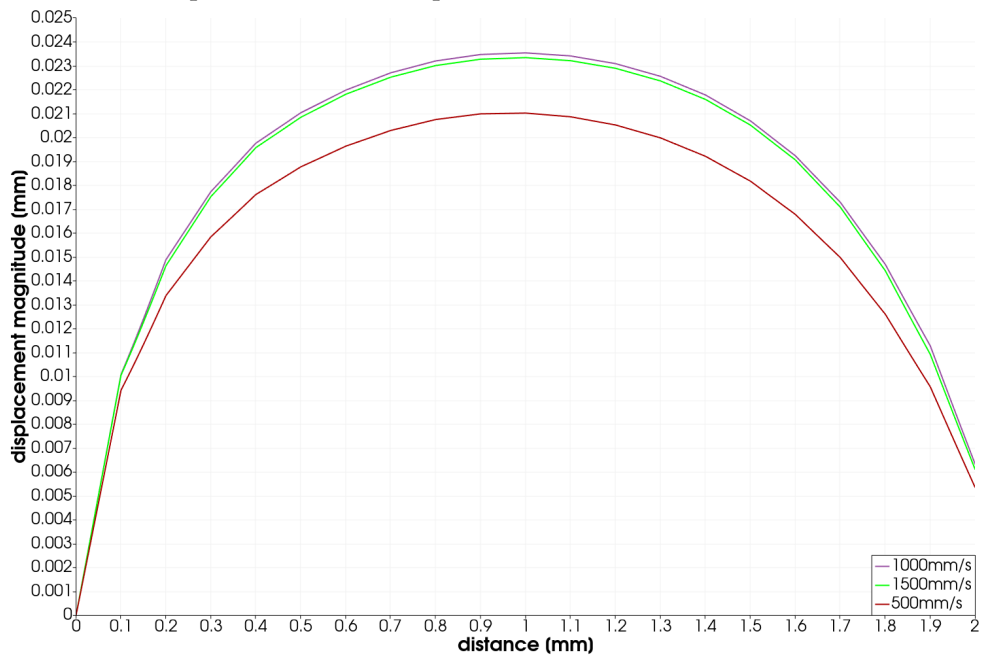
Laser Power

The initial laser Power of 300W has been increased to 400W as well as decreased to 200W . Figure 4.11 (a) shows that same as for laser scan speed the laser power affects the on plate residual stress. Again where the material does not yield the sensitivity is larger. Figure 4.11 (b) shows significant sensitivity to on plate displacement with a trend of higher displacement with lower power. The observed trend can be explained similarly to the effect found with varying the laser scan speed. Voxels that are given elevated IS values when using a low laser power are already being reset when using a higher laser power.

4. RESULTS



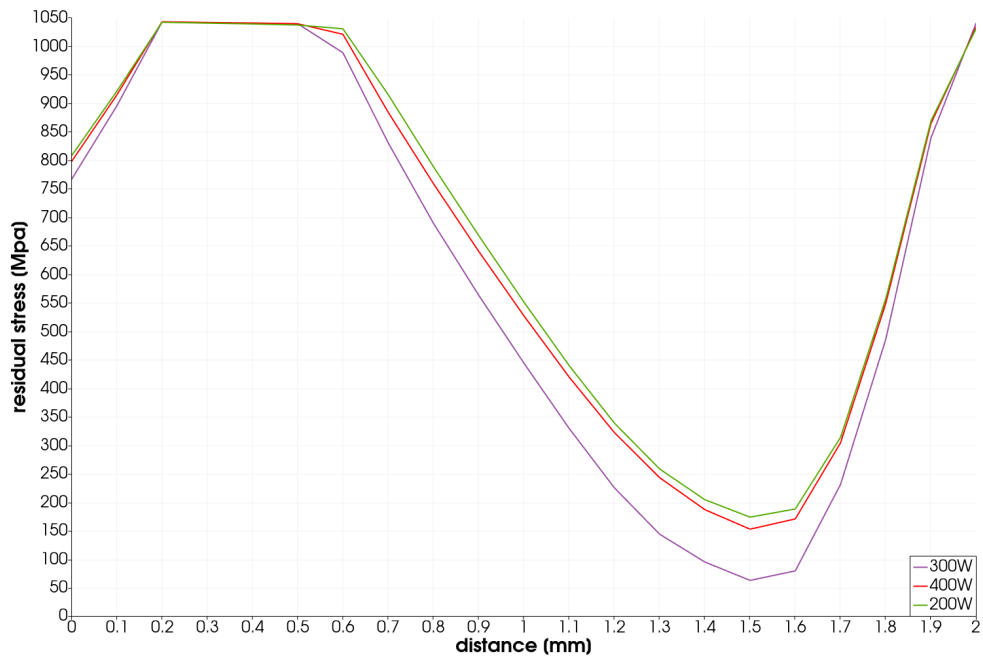
(a) on plate residual stress plotted over line from [1,1,0] to [1,1,2]



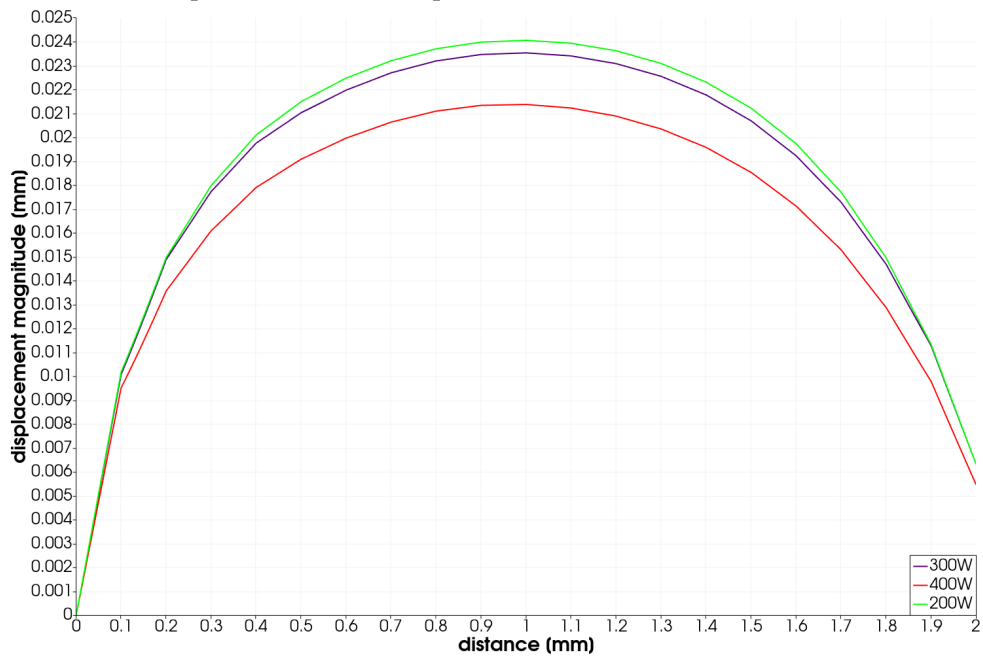
(b) on plate displacement plotted over line from [2,2,0] to [2,2,2]

Figure 4.10: AAP TS sensitivity to laser scan speed.

4.4. Sensitivity Analysis AAP



(a) on plate residual stress plotted over line from [1,1,0] to [1,1,2]



(b) on plate displacement plotted over line from [2,2,0] to [2,2,2]

Figure 4.11: AAP TS sensitivity to laser power.

Laser beam diameter

The laser beam diameter of $100\mu\text{m}$ has been increased to $110\mu\text{m}$ as well as decreased to $90\mu\text{m}$. From Figure 4.12 (a) and (b) can be seen that the tooth shaped stress field and edge displacement are not sensitive to a change in laser beam diameter. The displacement shows a trend of more displacement with increasing laser beam diameter. Francis et al. [20] showed that with increasing the laser beam diameter the melt pool becomes wider and shallower. However it is difficult to explain how this affects the thermal algorithm implemented in AAP since the sensitivity is only small.

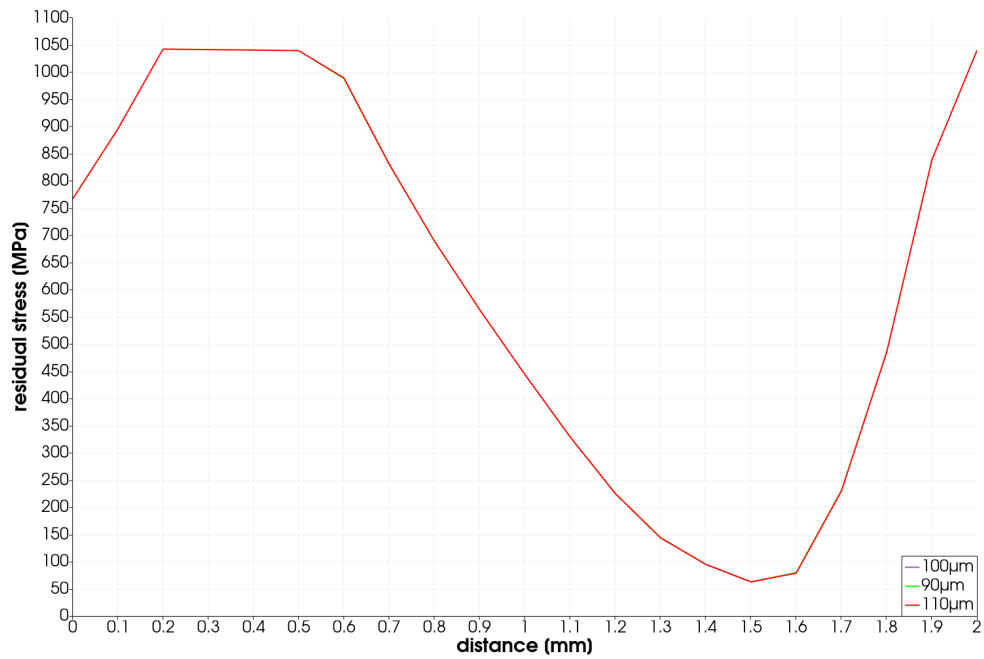
Hatch spacing

The initial hatch spacing of the stripe scan pattern of $100\mu\text{m}$ has been increased to $110\mu\text{m}$ and decreased to $90\mu\text{m}$. Figure 4.13 (a) shows that the hatch spacing affects the on plate residual stress where the material does not yield strongly with a trend of higher residual stress with larger hatch spacing. From Figure 4.13 (b) can be seen that the edge displacement shows a very small sensitivity to changes in hatch spacing where with larger hatch spacing the displacement becomes smaller. Dong et al. [21] showed that with increasing the hatch spacing the maximum temperature and heat accumulation reduce. A possible explanation for the found trend is that with increasing the hatch spacing there will be voxels that now fall just outside of the 40% threshold. Whereas the same voxels are still given elevated IS values with a lower hatch spacing.

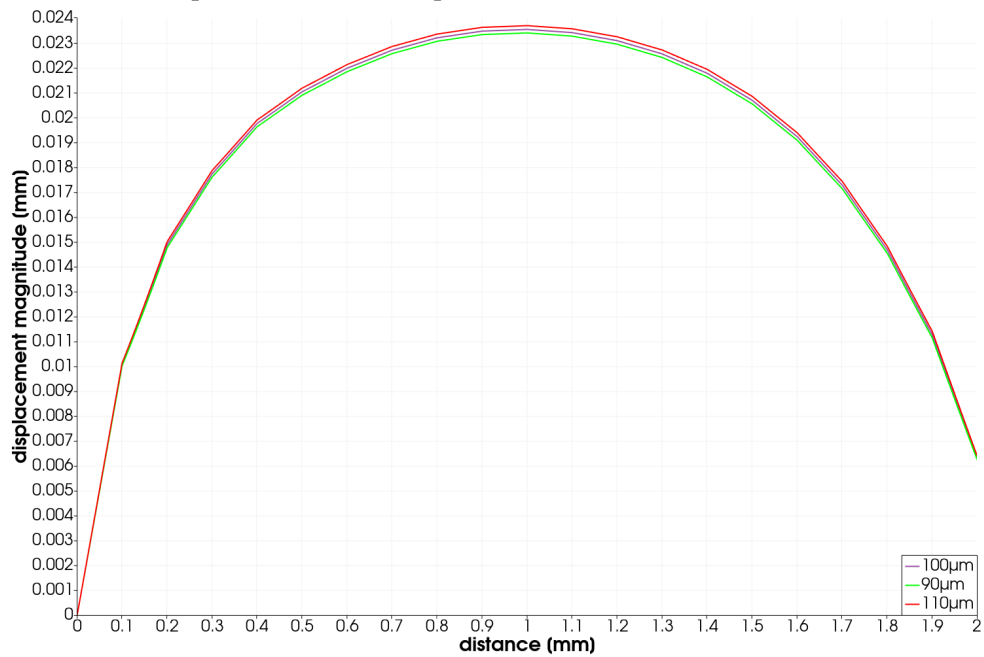
Base plate temperature

The initial base plate temperature of 80°C has been increased to 140°C as well as decreased to 40°C . Figure 4.14 (a) shows that there is no sensitivity to the tooth shaped stress field with varying base plate temperature. Figure 4.14 (b) shows that the edge displacement is sensitive to an increase in base plate temperature. A possible explanation that the base plate temperature of 140°C shows the highest on plate displacement is that by increasing the initial temperature of voxels there now will be voxels that just overcome the 40% threshold leading to more voxels with elevated IS values.

4.4. Sensitivity Analysis AAP



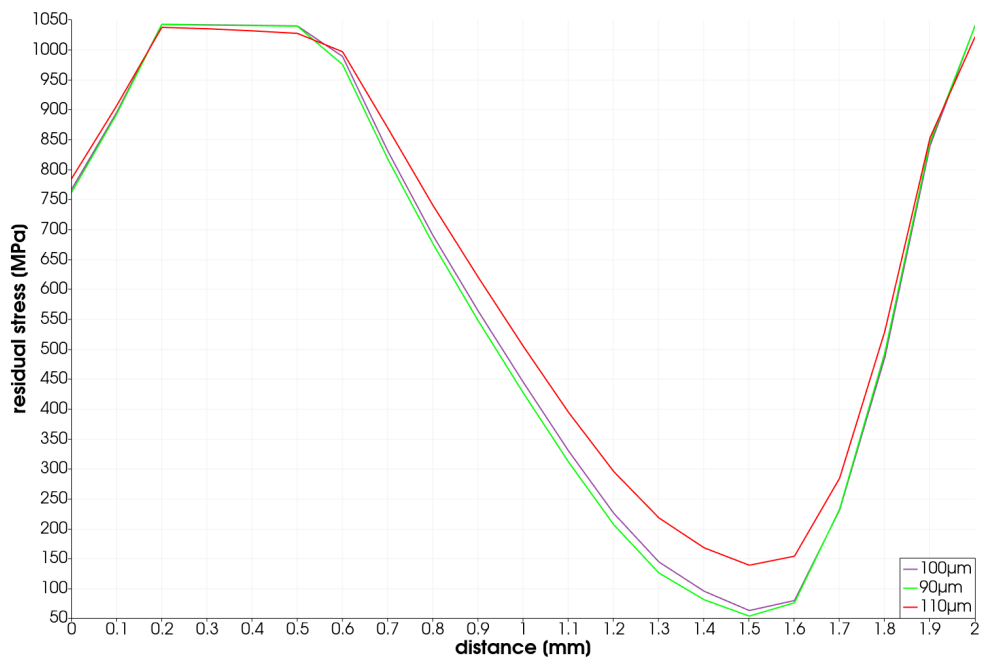
(a) on plate residual stress plotted over line from [1,1,0] to [1,1,2]



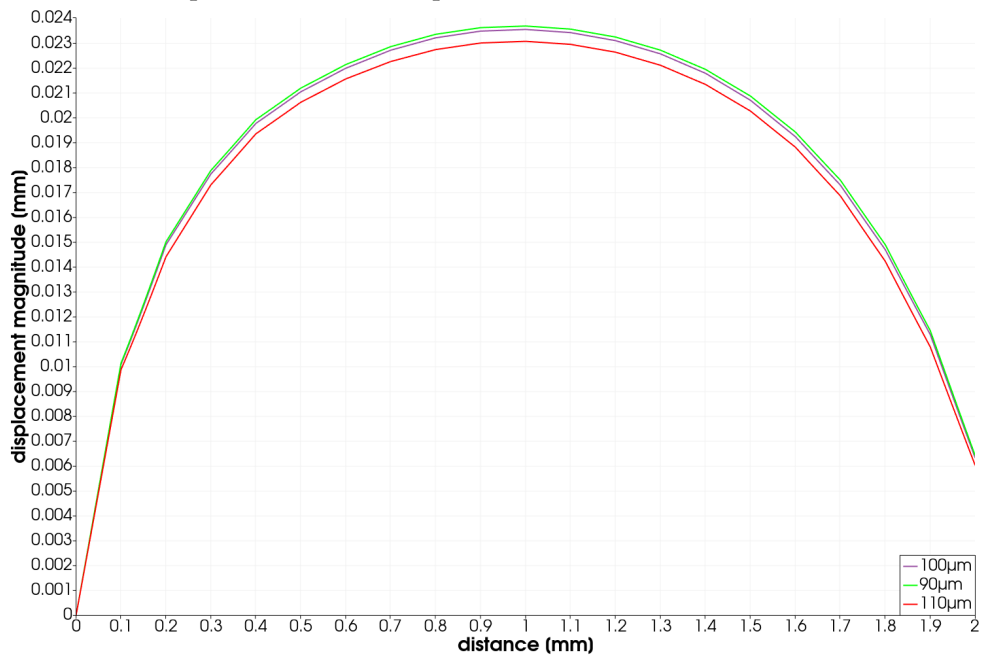
(b) on plate displacement plotted over line from [2,2,0] to [2,2,2]

Figure 4.12: AAP TS sensitivity to laser beam diameter.

4. RESULTS



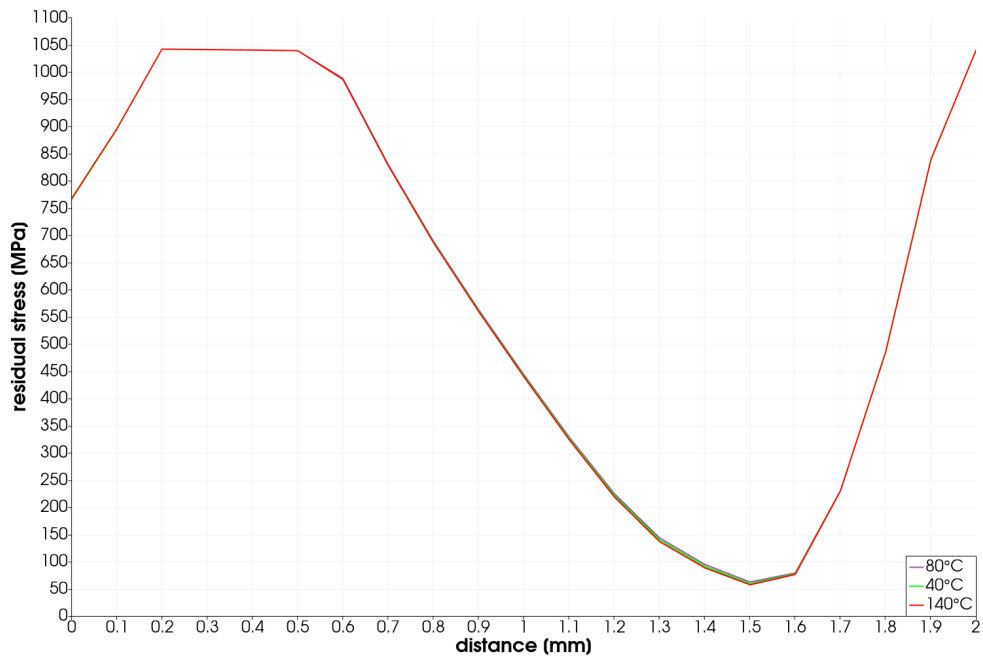
(a) on plate residual stress plotted over line from [1,1,0] to [1,1,2]



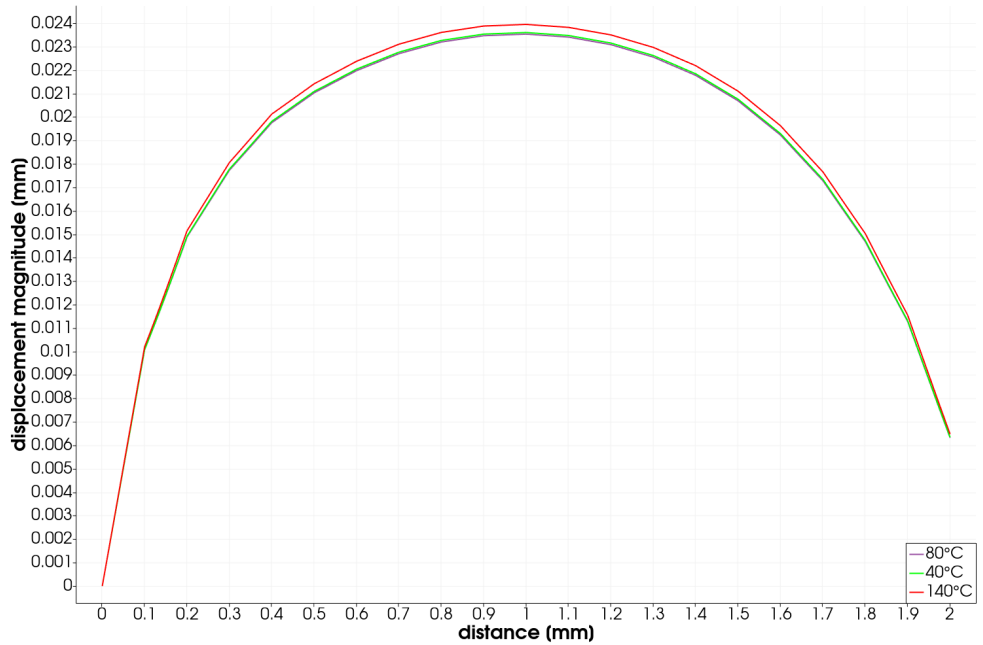
(b) on plate displacement plotted over line from [2,2,0] to [2,2,2]

Figure 4.13: AAP TS sensitivity to hatch spacing.

4.4. Sensitivity Analysis AAP



(a) on plate residual stress plotted over line from [1,1,0] to [1,1,2]



(b) on plate displacement plotted over line from [2,2,0] to [2,2,2]

Figure 4.14: AAP TS sensitivity to base plate temperature.

Conclusion and Outlook

The goal of this project was to investigate the implementation of IS in AAP as well as conduct a sensitivity analysis to the parameters of the three calculation modes AS, SPS and TS. To investigate the implementation a control isotropic and anisotropic IS model according to literature were implemented in Abaqus CAE.

AAP AS

- Follows the theory of the original IS method as found in literature [6, 3].
- Generally the voxel size should be defined through a voxel sensitivity study. AAP is optimized for part scale calculations. A voxel size of 1/4 of the smallest feature size will not always be sufficient for convergence especially in small scale parts.

AAP SPS

- Follows the theory of the original inherent strain method as applied in literature [6, 3] with the improvement of rotating the IS tensor of an element in the direction of average scan vector.

AAP TS

Since machine and powder parameters as a set are assumed to give unique SSF and ASF changing a parameter in the sensitivity analysis would also give different SSF and ASF values. Nonetheless a few trends have been observed.

- The Parameters laser beam diameter, hatch spacing and base plate temperature do not affect on plate displacement.
- The parameters laser power and laser scan speed affect both on plate residual stress and displacement.

Valuable further investigations would be to use a part scale test piece to compare the trends found in this work. To verify how the change in parameters affect the HAZ the change in melt pool dimensions with the varied parameters could be studied using for example Ansys Additive Science single bead or thermal history calculations. Also since a few parameters only show very small sensitivity in the TS calculation a further investigation in the SSF and ASF could be promising. It could be possible that a recalibration is not necessary for a subgroup of machine parameters.

Bibliography

- [1] Ian Gibson, David Rosen, Brent Stucker, and Mahyar Khorasani. *Additive manufacturing technologies*, volume 17. Springer, 2014.
- [2] Tarasankar DebRoy, HL Wei, JS Zuback, T Mukherjee, JW Elmer, JO Milewski, Allison Michelle Beese, A de Wilson-Heid, A De, and W Zhang. Additive manufacturing of metallic components—process, structure and properties. *Progress in Materials Science*, 92:112–224, 2018.
- [3] Nils Keller and Vasily Ploshikhin. New method for fast predictions of residual stress and distortion of am parts. 08 2014.
- [4] Jean-Pierre Kruth, Ludo Froyen, Jonas Van Vaerenbergh, Peter Mercelis, Marleen Rombouts, and Bert Lauwers. Selective laser melting of iron-based powder. *Journal of materials processing technology*, 149(1-3):616–622, 2004.
- [5] Pedro Alvarez, Joseba Ecenarro, Iñaki Setien, MS Sebastian, Alberto Echeverria, and Luka Eciolaza. Computationally efficient distortion prediction in powder bed fusion additive manufacturing. *Int. J. Eng. Res. Sci*, 2(10):39–46, 2016.
- [6] Matteo Bugatti and Quirico Semeraro. Limitations of the inherent strain method in simulating powder bed fusion processes. *Additive Manufacturing*, 23:329–346, 2018.
- [7] Saad A Khairallah and Andy Anderson. Mesoscopic simulation model of selective laser melting of stainless steel powder. *Journal of Materials Processing Technology*, 214(11):2627–2636, 2014.
- [8] Erik R Denlinger, Jeff Irwin, and Pan Michaleris. Thermomechanical modeling of additive manufacturing large parts. *Journal of Manufacturing Science and Engineering*, 136(6), 2014.

-
- [9] Dean Deng, Hidekazu Murakawa, and Wei Liang. Numerical simulation of welding distortion in large structures. *Computer methods in applied mechanics and engineering*, 196(45-48):4613–4627, 2007.
- [10] Yongtai Kim, Jaewoong Kim, and Sungwook Kang. A study on welding deformation prediction for ship blocks using the equivalent strain method based on inherent strain. *Applied Sciences*, 9(22):4906, 2019.
- [11] Ninshu Ma, Keiji Nakacho, Takahiko Ohta, Naoki Ogawa, Akira Maekawa, Hui Huang, and Hidekazu Murakawa. Inherent strain method for residual stress measurement and welding distortion prediction. In *ASME 2016 35th International Conference on Ocean, Offshore and Arctic Engineering*. American Society of Mechanical Engineers Digital Collection, 2016.
- [12] Hidekazu Murakawa, Dean Deng, Ninshu Ma, and Jiangchao Wang. Applications of inherent strain and interface element to simulation of welding deformation in thin plate structures. *Computational Materials Science*, 51(1):43–52, 2012.
- [13] Qian Chen, Xuan Liang, Devlin Hayduke, Jikai Liu, Lin Cheng, Jason Oskin, Ryan Whitmore, and Albert C To. An inherent strain based multiscale modeling framework for simulating part-scale residual deformation for direct metal laser sintering. *Additive Manufacturing*, 28:406–418, 2019.
- [14] Xuan Liang, Lin Cheng, Qian Chen, Qingcheng Yang, and Albert C To. A modified method for estimating inherent strains from detailed process simulation for fast residual distortion prediction of single-walled structures fabricated by directed energy deposition. *Additive Manufacturing*, 23:471–486, 2018.
- [15] Tea-Sung Jun and Alexander M Korsunsky. Evaluation of residual stresses and strains using the eigenstrain reconstruction method. *International Journal of Solids and Structures*, 47(13):1678–1686, 2010.
- [16] ANSYS Inc. Additive calibration guide.
- [17] ANSYS Inc. Additive user’s guide (print and science) release 2020r2.
- [18] Floriane Zongo, Charles Simoneau, Anatolie Timercan, Antoine Tahan, and Vladimir Brailovski. Geometric deviations of laser powder bed-fused alsi10mg components: numerical predictions versus experimental measurements. *The International Journal of Advanced Manufacturing Technology*, 107(3):1411–1436, 2020.

BIBLIOGRAPHY

- [19] Guglielmo Vastola, Gang Zhang, QX Pei, and Y-W Zhang. Controlling of residual stress in additive manufacturing of ti6al4v by finite element modeling. *Additive Manufacturing*, 12:231–239, 2016.
- [20] Zachary Ryan Francis. *The effects of laser and electron beam spot size in additive manufacturing processes*. PhD thesis, Carnegie Mellon University, 2017.
- [21] Zhichao Dong, Yabo Liu, Weibin Wen, Jingran Ge, and Jun Liang. Effect of hatch spacing on melt pool and as-built quality during selective laser melting of stainless steel: Modeling and experimental approaches. *Materials*, 12(1):50, 2019.



Eidgenössische Technische Hochschule Zürich
Swiss Federal Institute of Technology Zurich

Declaration of originality

The signed declaration of originality is a component of every semester paper, Bachelor's thesis, Master's thesis and any other degree paper undertaken during the course of studies, including the respective electronic versions.

Lecturers may also require a declaration of originality for other written papers compiled for their courses.

I hereby confirm that I am the sole author of the written work here enclosed and that I have compiled it in my own words. Parts excepted are corrections of form and content by the supervisor.

Title of work (in block letters):

Thermomechanical Simulation for Distortion and Residual Stress Prediction in SLM Parts: a Sensitivity Analysis

Authored by (in block letters):

For papers written by groups the names of all authors are required.

Name(s):

Müller

First name(s):

Fabian

With my signature I confirm that

- I have committed none of the forms of plagiarism described in the ['Citation etiquette'](#) information sheet.
- I have documented all methods, data and processes truthfully.
- I have not manipulated any data.
- I have mentioned all persons who were significant facilitators of the work.

I am aware that the work may be screened electronically for plagiarism.

Place, date

Rorbas, 04.06.2021

Signature(s)

For papers written by groups the names of all authors are required. Their signatures collectively guarantee the entire content of the written paper.